Scientia Iranica B (2022) 29(1), 13–25

Sharif University of Technology
Scientia Iranica
Transactions B: Mechanical Engineering
http://scientiairanica.sharif.edu

Angle design of stator-rotor blades for VLH axial flow turbine using surrogate-based optimization

N. Pholdee[a], W. Nuantong[b,*], S. Taechajedcadarungsri[c], and S. Bureerat[a]

a. *Sustainable Infrastructure Research and Department of Mechanical Engineering, Faculty of Engineering, Khon Kaen University, Khon Kaen, 40002, Thailand.*
b. *Department of Mechatronics Engineering, Faculty of Engineering, Rajamangala University of Technology Isan, Khon Kaen Campus, Khon Kaen, 40000, Thailand.*
c. *Department of Mechanical Engineering, Faculty of Engineering, Ubon Ratchathani University, Ubon Ratchathani, 34190, Thailand.*

Received 16 March 2019; received in revised form 22 December 2020; accepted 17 May 2021

KEYWORDS
Large eddy simulation;
Surrogate model;
Response surface;
Blade angle;
Optimization.

Abstract. The present study investigates the design of a very low head axial flow turbine using surrogate-based optimization. The design variables were blade angles between guide vanes and runner blades with the objective function of turbine efficiency. A Latin hypercube sampling method was initially used to design the experiment with thirty sampling points, and a large eddy simulation was modeled to analyze the flow for all sampling points. The correlation between the design variables and turbine efficiency was then evaluated using surrogate models while the optimal design variables were identified. In addition, several optimizers were employed to tackle the proposed problem and evaluate their performance. The optimal design of blade angles $\beta_1 - \beta_8$ of 10°, 20°, 30°, 40°, 25°, 45°, 55°, and 65° increased the turbine efficiency up to 89.87%. The approach of using surrogate modeling was proved to be very effective and simple in optimizing a design of blade angles of stator-rotor, and it could be used for designing any other new blades.

1. Introduction

Hydro energy generated from a large dam is very powerful with the ability to provide clean energy, hence practicable for electricity production with high potential as an alternative to coal and fossil fuels. However, the number of large dams in Thailand is not sufficient and their locations are not well distributed, especially in remote areas. One of interesting alternative energy sources is use of a Very Low Head (VLH) hydro turbine replacing a dam that needs high maintenance cost, flash floods, etc. The VLH hydro turbine is ecologically saved to operate within a small water reservoir such as a weir, a small waterfall, etc. Despite its several advantages, it cannot be totally used as a substitute for a large dam due to insufficient energy storage for a community. Moreover, the turbine needs a generator with high reliability and efficiency. For renewable energy supplement, an axial flow turbine is arguably the most popular owing to its high efficiency [1]. An optimum design of the turbine is therefore needed for maximum energy output.

Computational Fluid Dynamics (CFD) is one of the most powerful engineering tools for fluid flow analysis. Turbulence model simulation has been studied throughout the literature to design pumps, turbines [2–6], and other systems and according to the findings, the simulation results agreed well with those of the experiments. Here, CFD simulation of a Kaplan turbine was employed to predict the flow in a conical draft

*. *Corresponding author. Tel.: +669 3326 5205; Fax: +66 4 333 8869*
E-mail address: wee.nua16@gmail.com (W. Nuantong)

doi: 10.24200/sci.2021.53172.3099

tube directly below the runner cone using turbulence models of Unsteady Reynolds Average Navier-Stokes (URANS). The results were sufficiently precise when compared with the experimental results [7]. Large Eddy Simulation (LES) turbulence model also yielded good simulation results regarding the pressure on the blade on the pressure and suction sides, which also agreed well with the experimental results [8]. With simulation of axial flow hydraulic turbines, Sutikno and Adam predicted the turbine performance using the turbulence model $k-\varepsilon$ (Reynolds Average Navier-Stokes, RANS). The computational results were then compared with that from experiments as well as that of the power output with less than 5% difference [9]. Cheng et al. compared two turbulence models obtained from LES and RANS that were used to simulate the turbulent flow over a cube matrix. When comparing the experimental results with simulation results, LES was superior to RANS [10]. Su et al. simulated the interior flow characteristics of hydraulic turbines using a combination of LES with the Smagorinsky-Lilly model and RANS with $k-\varepsilon$ turbulence model. The LES results were more accurate than that obtained from the $k-\varepsilon$ to predict the overall performance [11]. Therefore, this study selected the LES method with Smagorinsky-Lilly model for fluid flow analysis to reduce the effect of unsteadiness and gain the required accuracy for turbine simulation.

Design of fluid machinery based on CFD has been widely reported in the literature. For example, a suitable airfoil section for blades of a horizontal axis hydrokinetic turbine was studied based on CFD in [12]. The effects of the number of blades, initial angle of attack of the airfoil, twist angle of the blade, and chord length on the power coefficient of the airfoil, pressure coefficient, and cavitation number of high-head turbine were investigated based on CFD and real experimental study. In good agreement with the experimental results, the results confirmed that the design improvement of the turbine blade through CFD method was accurate [13]. The structural optimization of the cover of a high-head axial hydro turbine was also investigated based on one-way fluid-structure interaction computation using Finite Element Analysis (FEA) and CFD [14]. Similarly, in the blade design of a horizontal-axis hydrokinetic turbine, a hybrid approach which was a combination of Blade Element Momentum (BEM) theory, Genetic Algorithm (GA), CFD, and FEA techniques was employed to improve the blade by optimizing chord lengths and blade twist angles. According to this study, the power coefficient of the turbine increased by 17% [15]. The Francis carbon blades were studied using FEA to design blades as thin as possible with reduced weight and high strength [16]. Optimization of Francis turbine blades for a low-head runner case study was also developed based on a multi-fidelity design algorithm [17]. Optimization of a VLH turbine blade based on XFOIL was reported in [18] to minimize the drag-to-lift ratio. To increase turbine efficiency, the runner blade and draft tube were designed for optimization using the CFD and GA [19]. In addition, the optimum design of an axial flow fan was presented in [20] while using CFD and vortex law for fluid flow analysis. Similarly, optimization of air-turbine blades for increasing torque was presented in [21]. In this study, CFD was used as a tool for fluid flow analysis with the design variables, namely blade tip width and angle of turbine blade. In addition, surrogate assisted optimization is wieldy used for axial flow turbine optimization to overcome the expensive computation problems such as optimization of a sweep blade of a Wells turbine [22], turbomachinery blade design in [23,24], a pump and an axial compressor [25,26], a micro gas turbine [27], and a high-head pump turbine [28].

Nowadays, while designing a hydro turbine, most engineers focus on increasing the capability of VLH hydropower. An axial flow turbine was proved to be appropriate for low head water sources [1]. The turbine set consists of guide vanes and runner blades that significantly affect the turbine performance; both assemblies are the key parts in energy conversion. Therefore, optimization of a VLH axial flow turbine through designing the guide vanes and runner blades is interesting. According to the literature, an optimization study on a hydro turbine puts its main focus on a high-head turbine; however, the VLH turbine has been rarely studied.

In the present study, optimization of a VLH hydro turbine was performed based on a combination of a surrogate model and a Meta-Heuristic (MH) optimizer. The optimization problem was posed to maximize the turbine efficiency with the blade angles as the design variables. In this regard, several MHs along with response surface and kriging surrogate models were employed, and CFD was used for real objective function calculation.

2. Optimization problem formulation

This study aims to optimize a three-dimensional axial flow turbine model, as shown in Figure 1. The operating conditions of the local site were defined with a water head level of two meters and the flow rate of 5 m^3/s. These values were used to solve the runner diameter of the turbine given in Eq. (1):

$$Q = \left[\frac{\pi D^2}{4}\right] \times \left[1 - \left(\frac{D_h}{D}\right)^2\right] \times \sqrt{2gH}. \quad (1)$$

The diameter ratio of hub to tip ($\frac{D_h}{D}$) for an axial flow turbine ranges typically from 0.4 to 0.55 [29]. In

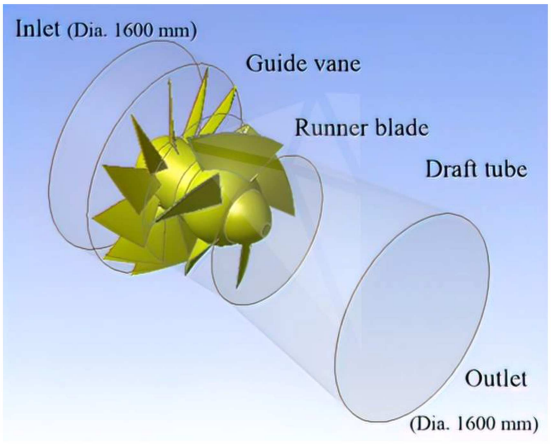

Figure 1. Geometry of an axial flow turbine.

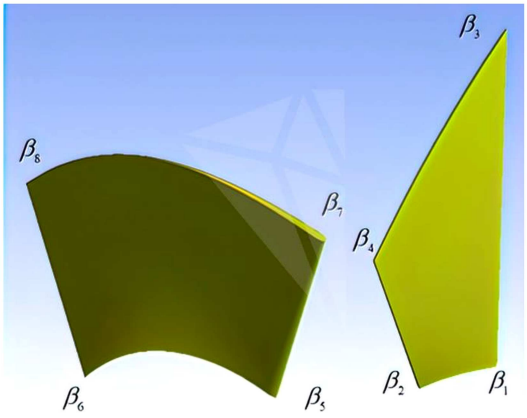

Figure 2. Angle positions of the guide vane and the runner blade.

this research, the average value of 0.48 was assumed to calculate the blade diameter. The turbine blade is characterized by a tip diameter of 1.15 meters and a hub diameter of 0.55 meters for 5 blades and 12 guide vanes, respectively. The geometry of an axial flow turbine was created using the ANSYS Workbench software. The region around the turbine is composed of five parts namely inlet, guide vane, runner blade, draft tube section, and outlet. Both the inlet and outlet of the tube were characterized by a diameter of 1600 mm.

The guide vanes and runner blades were the core components used for improving the performance of an axial flow turbine. The design variables of the blade angles between guide vane and runner blade at the leading and trailing edge positions of the hub and blade tip were taken into account to assess the turbine efficiency. The guide vane angles β_1 and β_2 in the hub position were defined with the tip angles β_3 and β_4, respectively. Similarly, the runner blade angles β_5 and β_6 in the hub position were defined with the tip angles β_7 and β_8, respectively. Figure 2 presents a schematic demonstration of the blade angles between guide vane and runner blade.

The thickness values of the guide vanes on the leading and trailing edges were 10 mm and 5 mm, respectively, and those of the runner blade in the hub and tip positions range from 5 to 20 and 5 to 15 mm, respectively, from the leading edge to the trailing edge. The values of the initial thickness of both guide vane and the runner blade were defined based on the constraints on materials and manufacturing processes.

To optimize the blade shape, the objective function is posed to maximize the turbine efficiency when the optimization which is formulated as a minimization problem can be expressed as follows:

$$\min: \ 1 - \frac{\eta(\beta)}{100}, \tag{2}$$

subjected to:

$$L_i \leq \beta_i \leq U_i,$$

where $\eta(\beta)$ is a function of the turbine efficiency and $\beta = (\beta_1, \cdots, \beta_8)$ represent the design variables detailed in Figure 2; L_i and U_i are the lower and upper bounds of the angles β_i, respectively. The CFD technique (LES) was also introduced to determine the turbine efficiency.

3. Computational fluid dynamics

3.1. Governing equations

The present study employed the LES turbulence model to simulate the fluid flow in a hydro turbine system, proven to be reliable in studies of Su et al. [11] and Altimemy et al. [30]. The LES method was explicitly resolved such that eddy smaller than the grid size was simulated by implementing a Subgrid-Scale (SGS) model. A large-scale structure was solved using the Navier-Stokes equations through a filtering approach defined as:

$$\frac{\partial \bar{u}_j}{\partial x_j} = 0, \tag{3}$$

$$\frac{\partial \bar{u}_i}{\partial t} + \frac{\partial \bar{u}_j \bar{u}_i}{\partial x_j} = -\frac{1}{\rho}\frac{\partial \bar{p}}{\partial x_i} + \frac{\partial}{\partial x_j}\left(\upsilon \frac{\partial \bar{u}_i}{\partial x_j}\right) - \frac{\partial \tau_{ij}}{\partial x_j}, \tag{4}$$

where $\bar{u}_j = u_j - u'_j$ is the filtered velocity vector in which the overbar stands as a filtering operator, ρ the density of the fluid, $\bar{p}$ the resolved pressure, t the time, and $\tau_{ij} = \overline{u_i u_j} - u_j u_i$ the subgrid shear stress evaluated using SGS models. Through the Boussinesq hypothesis, the SGS turbulent stress is defined by:

$$\tau_{ij} = \frac{1}{3}\tau_{kk}\delta_{ij} - 2\mu_t \bar{S}_{ij}, \tag{5}$$

where δ_{ij} is the Kronecker delta, μ_t the SGS eddy viscosity, τ_{kk} the SGS stress, and $\bar{S}_{ij}$ the strain-rate tensor in relation to the following:

$$\bar{S}_{ij} = \frac{1}{2}\left(\frac{\partial \bar{u}_i}{\partial x_j} + \frac{\partial \bar{u}_j}{\partial x_i}\right). \quad (6)$$

The Wall-Adapting Local Eddy-viscosity (WALE) method was modeled to solve the SGS eddy-viscosity through the following relations:

$$\mu_t = L_S^2 \frac{\left(S_{ij}^d S_{ij}^d\right)^{3/2}}{\left(\bar{S}_{ij}\bar{S}_{ij}\right)^{5/2} + \left(S_{ij}^d S_{ij}^d\right)^{5/4}}, \quad (7)$$

$$S_{ij}^d = \frac{1}{2}\left[\left(\frac{\partial \bar{u}_i}{\partial x_j}\right)^2 + \left(\frac{\partial \bar{u}_j}{\partial x_i}\right)^2\right] - \frac{1}{3}\delta_{ij}\left(\frac{\partial \bar{u}_k}{\partial x_k}\right)^2, \quad (8)$$

$$L_s = \min\left(kd, C_s V^{1/3}\right), \quad (9)$$

where L_s is the mixing length for SGS, k the Von Kármán constant, d the shortest distance to the nearest wall, C_s the WALE constant of 0.325, and V the mesh cell volume. The eddy-viscosity is solved nearly zero in areas close to walls without any application of the damping function [11,30].

3.2. CFD simulation

A moving mesh was utilized to simulate the flow in the turbine. The LES method with the Smagorinsky-Lilly model is an efficient turbulence model with acceptable results in simulating the flow field in the work of hydro-turbines [11]. First, it was used in this study to evaluate the flow effect on the turbine blade. CFD analysis was then carried out using the ANSYS Fluent software for turbine simulations.

The results obtained from CFD validation, prior to their application in this study, were simulated and compared with the experimental results obtained from Ramos et al. [31]. Initially, the turbine was defined with a diameter of 100 mm and five blades. The turbine blade profiles were described by the blade angles in the experiment [31]. In the proposed approach, the validation results of CFD simulation were in good agreement with those from experiment, as shown in Figure 3. It should be noted that the turbine in [31] is merely used for validating the CFD simulation accuracy. It is different from the turbine optimized in this study. However, operation of the validated axial flow turbine has similar conditions to our turbine, which is a VHL axial flow turbine.

Figure 3 presents a comparison between the CFD simulation and experimental results as the plots of turbine efficiency versus flow rate. The turbine efficiency from experiment was found to be more scattering than those from CFD simulation at the same flow rate.

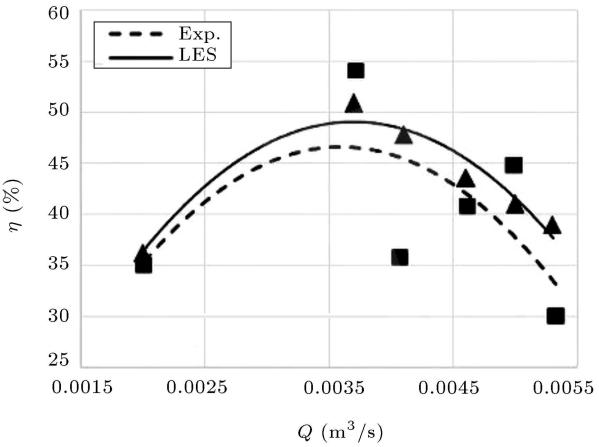

Figure 3. Computational Fluid Dynamics (CFD) validation with experimental results.

However, the trending average on the curves of both efficiency data sets was similarly distributed. The turbine efficiency from the experimental data set on the average curve was lower than that of the CFD simulation data set mainly due to the energy loss and experimental uncertainties in the real system, which was neglected in the simulation. According to the findings, the maximum turbine performance of both CFD and experiment was at a flow rate of 0.0037 m^3/s. The maximum efficiency values of the turbine from CFD simulation and experiment were 50.94% and 54%, respectively. The relative error between the maximum efficiencies of both approaches was 5.7%.

Accordingly, the CFD simulation through the LES method with the Smagorinsky-Lilly model is an efficient turbulence model that can be used to represent the real testing results of the hydro turbine. As a result, the CFD approach is used for function evaluations of the training points generated by means of design of computational experiment. In addition, it can be used to check the final optimum solution obtained from surrogate-assisted optimization. Surrogate models are generally used in a wide variety of real-world applications. Neural network and support vector regression models are used to estimate velocity and flow depth variables at a sharp bend of 60° [32]. A response surface model was used to analyze the data and find behavioral equations on the remolded clayey samples mixed with gasoil to evaluate their geotechnical properties [33]. A radial basis function model was also used for optimization of highway guardrails [34], and the kriging model was employed to quantify uncertainties in the design of an aircraft wing structure [35]. Such models are regarded as the numerical tools for engineers.

3.3. Mesh generation and boundary conditions

As shown in Figure 1, four computational domains are defined as inflow, guide vane, runner blade, and outflow domain. The solid domain of the runner blade rotates

at 200 rpm and the other domains are kept constant. Unstructured 3D tetrahedral mesh was selected in this study due to the complex geometries of the axial flow turbine. The boundary conditions for simulating the flow are defined as follows.

The total and static pressures are zero for the inlet and outlet flows. The guide vane, runner blade, and other parts of the turbine are defined as the surface walls where the wall of the runner blade is rotating.

The initial flow was dependent on the constraints on the local installation site. Therefore, the water head was set at two meters and the volume flow rate was 5 m^3/s for the inlet pressure, with the runner blade rotating at a speed of 200 rpm. The time revolution of the runner was 0.3 sec per round, and the simulation was performed for at least 1.6 flow cycles. To reach a robust solution, the pressure-velocity coupling scheme was employed in this study [36]. A standard scheme for pressure interpolation [11] and Quadratic Upwind Interpolation for Convective Kinetics (QUICK) scheme [37] were also taken into consideration. Further, momentum interpolation was also utilized. The transient formulation was set in a second-order implicit scheme, while the residual criteria were controlled at 10^{-5}.

The mesh validation was initially performed to ensure that the results of the turbine performance would be identified as almost constant. As shown in Figure 4, the turbine efficiency decreased upon increasing the mesh density. The numbers of grid elements were between 3.02-8.91 million. The convergence of the results was defined when the number of elements was higher than 5.0 million. In this study, the grid elements of approximately 6.01 million were considered to shorten the numerical time. Obviously, the efficiency of the turbine was almost constant for the number of grid elements between 5.00 and 8.91 million. The difference in turbine efficiency for the numbers of grid elements of 6.01 and 7.06 million was 0.09%.

As shown in Figure 5(a) and 5(b), the pressure distribution on the runner blade using 6.01 and 7.06 million mesh elements is almost the same.

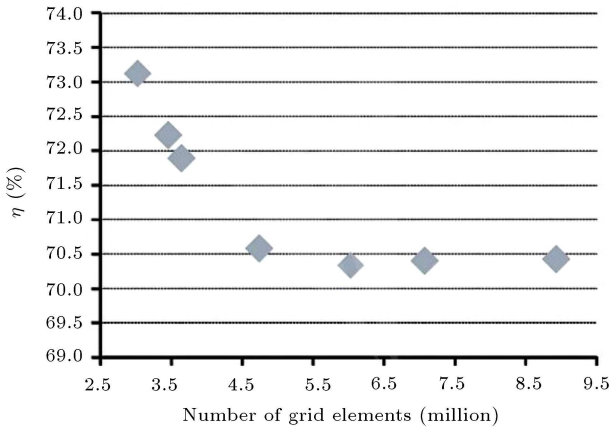

Figure 4. Mesh validation results.

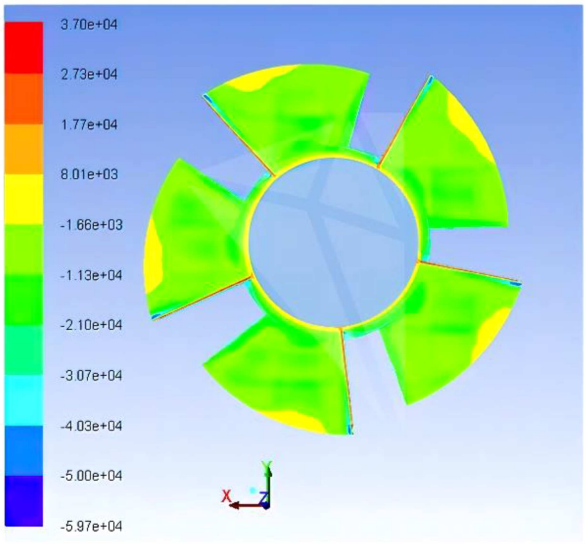

(a) Pressure side with 6.01 million

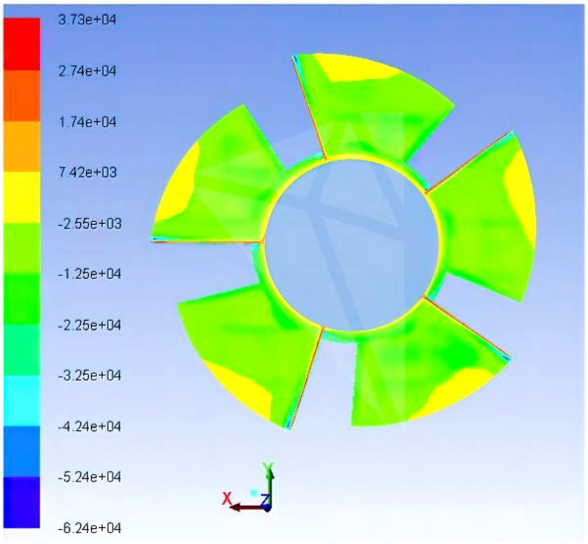

(b) Pressure side with 7.06 million

Figure 5. Pressure contours of the runner blade.

4. Surrogated assisted optimization

A surrogate-assisted optimization technique was proposed for the optimization problem with expensive objective function evaluations due to high fidelity computation. In this case, performing optimization using the real expensive function evaluation is made impossible. The main idea behind using surrogate-assisted optimization is that the real expensive evaluation is approximated by a constructed inexpensive function while performing an optimization process based on the inexpensive function. The conventional process of the surrogate-assisted optimization consists of three main

steps. Firstly, a set of sampling points is generated throughout the design domain using Design Of Experiment (DOE) technique. Then, the objective function value of each sampling point is calculated based on the real expensive function evaluation. Next, a surrogate model is constructed and optimization is performed based on the constructed inexpensive function or a surrogate model. Followed by achieving an optimum solution, its real function value is calculated using the expensive function evaluation, which is referred to as the CFD simulation in this study.

For the proposed optimization of the turbine blades, a conventional surrogate-assisted optimization technique is used. Latin Hypercube Sampling (LHS) technique is firstly used for generating a set of sampling points. Then, CFD is employed to evaluate the real objective function of each sampling point. Surrogate models based on polynomial response surface and kriging models are then constructed and optimization is performed based on the constructed surrogate models. Several MH optimizers along with a linear programing optimizer are used to solve the proposed optimization problem.

4.1. DOE by LHS technique

M sampling points using LHS can be generated by dividing the bound $[L_i, U_i]$ into M subintervals based on the following equation:

$$L_{ij} = L_i + \frac{(j-1)(U_i - L_i)}{M}, \tag{10}$$

$$U_{ij} = L_i + \frac{j(U_i - L_i)}{M}, \tag{11}$$

where L_{ij} and U_{ij} are the lower and upper bounds of the subinterval j of the ith design variable, respectively. For each subinterval, a sampling point is generated using the equation leading to M sampling points.

$$X_{ij} = L_{ij} + (U_{ij} - L_{ij}) \cdot \text{rand}. \tag{12}$$

Finally, the elements of each column of X are randomly permuted [38]. Table 1 shows 30 sampling points generated using LHS for the proposed hydro turbine blade optimization problem with eight design variables. The lower and upper bounds for each design variable are also presented in this table. Note that the lower

Table 1. Sampling of DOE.

Sampling	DOEs of blade angles (deg)							
	β_1	β_2	β_3	β_4	β_5	β_6	β_7	β_8
L_i	10	20	30	40	25	35	45	55
U_i	20	30	40	50	35	45	55	65
1	11.2	22.7	34.8	49.2	29.2	42.3	46.7	55.5
2	17.5	21.1	36.9	48.1	29.6	39.3	48.4	61.6
3	12.1	29.7	38.1	44.5	33.6	38.7	45.8	57.0
4	16.2	20.1	32.5	44.0	26.6	42.9	47.3	59.7
5	18.0	20.8	31.4	40.4	27.8	44.4	50.5	63.6
6	19.9	24.4	32.8	46.7	27.5	36.0	50.8	58.5
7	15.9	25.1	33.1	42.8	25.9	43.6	51.1	56.5
8	19.4	26.7	34.5	44.9	34.7	44.8	45.3	59.3
9	18.4	28.5	35.4	42.3	34.4	39.6	48.1	59.5
10	19.0	25.6	32.2	48.4	26.1	43.8	47.6	63.7
11	17.0	26.4	36.4	47.4	32.5	36.3	53.5	62.2
12	13.2	21.9	33.8	41.8	31.3	41.1	53.8	57.9
13	17.9	20.4	38.4	49.0	30.6	43.0	52.0	64.1
14	14.2	29.1	31.7	49.8	34.1	35.5	54.9	60.6
15	10.2	24.0	35.3	46.8	30.1	40.3	49.2	57.3
16	12.0	28.1	30.7	43.7	28.3	38.1	50.3	56.0
17	14.7	27.0	38.9	43.5	31.6	40.8	50.0	60.7
18	15.3	23.7	31.2	40.1	28.9	41.6	47.8	62.7
19	16.4	23.0	39.7	45.7	27.1	36.7	45.4	58.7
20	10.5	23.4	37.1	46.2	33.7	40.0	53.2	62.5
21	12.7	22.4	33.4	49.4	33.0	44.3	54.3	61.0
22	13.9	24.7	39.0	42.5	26.9	36.5	51.6	60.1
23	11.3	28.9	34.1	47.0	25.7	41.7	46.5	63.3
24	15.6	26.3	39.6	40.9	31.7	37.2	48.9	64.9
25	11.0	26.0	30.9	41.6	30.9	42.5	54.7	55.1
26	19.0	29.4	30.2	45.1	29.8	40.7	49.5	58.1
27	14.7	27.8	37.5	45.5	25.3	35.3	52.2	57.5
28	16.8	27.5	36.1	43.2	32.1	38.0	52.4	64.7
29	12.4	21.5	35.8	41.0	28.5	38.6	46.0	61.7
30	13.4	22.1	37.9	47.8	33.1	37.5	52.7	56.2

and upper bounds used in this study are set based on the available values reported in [3,39–41].

After generating a set of sampling points based on LHS, the turbine performance criteria including turbine efficiency, torque, flow rate, and total head for all sampling designs for each sampling are evaluated based on CFD, the results of which are given in Table 2. According to this table, the maximum efficiency of the turbine of these 30 sampling points is 85% with the blade angles $\beta_1 - \beta_8$ of 18°, 20.8°, 31.4°, 40.4°, 27.8°, 44.4°, 50.5°, and 63.6°, respectively.

4.2. Surrogate model

After achieving the desired turbine performance, the correlation between the design variables of blade angles ($\beta_1 - \beta_8$) and turbine efficiency is presented in a scatter plot in Figure 6. As observed in this figure, there is no correlation between the blade angles themselves while all of the blade angles appear linearly correlated to the turbine efficiency. In addition, Pearson's correlation method is used to examine the correlation between the turbine efficiency and blade angles ($\beta_1 - \beta_8$). The correlation between the turbine efficiency and blade angles ($\beta_1 - \beta_8$) is 0.1137, −0.3999, −0.2498, −0.0941, −0.102, 0.2426, 0.4022, and 0.5448, respectively. The correlation between the design variables of β_1, β_3, β_4, β_5, and β_6 with the turbine efficiency is quite low; however, the β_2 and β_7 are of low correlation and β_8 has a medium-rated correlation with the turbine efficiency. Moreover, while the design variables of β_2, β_3, β_4, and β_5 show an inverse correlation with the turbine efficiency, β_1, β_6, β_7, and β_8 present a direct correlation.

Three surrogate models were constructed based on the sampling points in Tables 1 and 2. The first and second models were constructed based on the first-order polynomial function, expressed as Eq. (13):

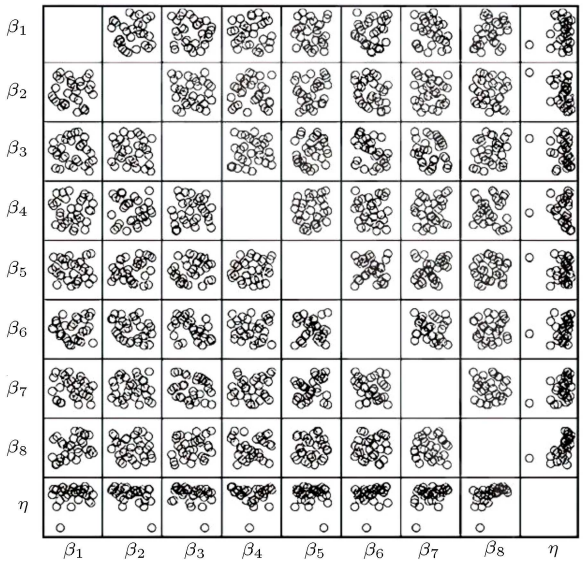

Figure 6. Scatter plot of input-output data.

Table 2. Computational Fluid Dynamics (CFD) results of sampling models.

Sampling	Q (m^3/s)	H (m)	τ (Nm)	η (%)
1	4.66	1.78	2735.50	70.34
2	4.29	1.70	2732.88	79.93
3	4.50	1.75	2025.70	55.09
4	4.65	1.82	3251.22	82.14
5	4.38	1.95	3397.82	85.00
6	4.55	1.74	2920.30	78.94
7	4.70	1.83	3236.36	80.58
8	4.47	1.85	2826.69	73.08
9	4.57	1.84	3095.68	78.50
10	4.15	1.81	2898.62	82.30
11	4.12	1.71	2667.42	80.82
12	4.66	1.84	3299.77	82.41
13	3.99	1.85	2863.05	83.08
14	4.25	1.83	3003.90	82.67
15	4.64	1.80	3082.63	78.84
16	4.81	1.79	3011.83	74.86
17	4.36	1.78	2945.83	81.03
18	4.56	1.88	3388.80	84.30
19	4.60	1.71	2769.25	75.37
20	4.20	1.84	3007.68	83.13
21	4.19	1.87	3096.75	84.35
22	4.45	1.70	2805.96	79.29
23	4.25	1.78	2934.99	83.11
24	4.18	1.77	2791.82	80.66
25	4.82	1.85	3422.22	82.10
26	4.56	1.83	2900.36	74.28
27	4.50	1.80	2659.80	70.20
28	4.08	1.80	2844.45	82.61
29	4.61	1.76	3078.03	81.20
30	4.54	1.69	2779.34	77.31

$$\eta(\beta) = k_0 + k_1\beta_1 + k_2\beta_2 + \cdots + k_8\beta_8, \tag{13}$$

where $\eta(\beta)$ is a function of the turbine efficiency, and the terms $k_0, k_1, k_2, \cdots, k_8$ are the regression coefficients. While the first response surface function is constructed using all 30 sampling points, the second response surface model is constructed based on only

nine sampling points, which is the minimum sampling required for eight design variables. Of note, these nine sampling points used for constructing the second response surface model were selected based on a K-mean clustering technique from the 30 sampling points. The linear response surface functions obtained from 30- and 9-sampling-point sets are shown in Eqs. (14) and (15):

$$\begin{aligned}\eta_f =& 13.8742 - 0.108\beta_1 - 0.6385\beta_2 - 0.5954\beta_3 \\ & - 0.1996\beta_4 - 0.2346\beta_5 + 0.1042\beta_6 \\ & + 0.8623\beta_7 + 1.2021\beta_8, \end{aligned} \tag{14}$$

$$\begin{aligned}\eta_f =& 31.6901 - 0.113\beta_1 - 0.0202\beta_2 - 0.3938\beta_3 \\ & - 0.0314\beta_4 - 0.0837\beta_5 + 0.3064\beta_6 \\ & + 0.3132\beta_7 + 0.6793\beta_8. \end{aligned} \tag{15}$$

In addition, the third surrogate model was constructed using the kriging model. The DACE MATLAB kriging toolbox was used for the kriging model construction while utilizing Gaussian correlation function with a linear regression model.

4.3. Optimizers used and their parameter setting

To solve the proposed optimization problem based on the three surrogate models, several MH optimizers and linear programming were used. The employed MHs and their parameter settings are detailed in the following:

- *Artificial Bee Colony (ABC) [42]:* The number of food sources for the employed bees was set to $n_p/2$. A trial counter to discard a food source was 100;
- *Real Code Ant Colony Optimization (ACOR) [43]:* The parameter settings were $q = 0.2$ and $\xi = 1$;
- *Differential Evolution (DE) [44]:* The DE/best/2/bin strategy was used. A scaling factor, crossover rate, and probability of choosing elements of mutant vectors were 0.5, 0.7, and 0.8, respectively;
- *Particle Swarm Optimization (PSO) [45]:* The starting inertia weight, ending inertia weight, cognitive learning factor, and social learning factor were calculated as 0. 5, 0.01, 2.8, and 1.3, respectively;
- *Grey Wolf Optimizer (GWO) [46]:* There was no required parameter setting
- Moth-Flame Optimization Algorithm (MFO) [47]: The constant parameter b was set to 1 while other parameters were iteratively adopted.

Linear programming was used to solve the first and second surrogate models as they were linear functions while the MHs were employed to solve the third surrogate model constructed from the kriging model. For each MH, since the method employs randomization, the problem was tackled for 30 optimization runs while the results of various MHs were compared in terms of search convergence and consistency. The best results obtained from the kriging-assisted MHs were then compared with those from the two linear models, which were solved using the linear programming. For each MH, population size and number of iterations were set to 20 and 200, respectively.

5. Results and discussion

Followed by performing optimization based on the three surrogate models, MHs performance in solving the proposed optimization problem through kriging model was evaluated. After performing 30 optimization runs for each MH, the results are shown in Table 3. According to this table, the mean objective function values (Mean) were utilized to measure the search convergence, and the Standard Deviation of objective function values (STD) was aimed at measuring the search consistency. It was found that all MHs were characterized by somewhat similar search convergence and consistency except for the DE and PSO, known as two worse algorithms in terms of search convergence and consistency. However, all of the MHs obtained the same minimum objective function values of 0.01434. Figure 7 shows the search history of the best run for

Table 3. Results of 30 optimization runs for each MHs.

MHs	Mean	STD	Min	Max
ABC	0.01434	0	0.01434	0.01434
ACOR	0.01434	0	0.01434	0.01434
DE	0.014688	0.001903	0.01434	0.024765
PSO	0.029062	0.02069	0.01434	0.097341
GWO	0.01434	0	0.01434	0.01434
MFO	0.01434	0	0.01434	0.01434

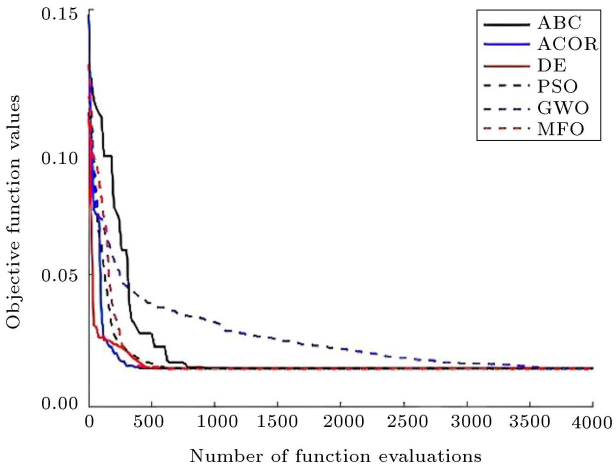

Figure 7. Search history of the best run for the all MHs.

each MH. As observed in this figure, DE, ACOR, PSO, and MFO have faster convergences from the beginning and ACOR is the best algorithm that can first converge to the optimum. Based on this investigation, it can be concluded that ACOR is the most efficient algorithm for the proposed optimization of a VLH turbine based on the kriging model.

The best result obtained using kriging-assisted MHs was compared with those from the two remaining linear surrogate models solved by linear programming. After optimization of the two remaining linear surrogate models, the results are shown in Table 4. Here, η_f is the turbine efficiency calculated through a surrogate model and η_{optCFD} is the efficiency obtained from actual function evaluations of CFD. Obviously, similar optimum points were obtained from all chosen models. The accuracy rates of the 30-point linear, 9-point linear, and kriging models at optimum, compared to that of CFD analysis, were 8.82, 0.32, and 8.82%, respectively. The optimal turbine efficiency based on CFD was measured as 89.87%. Since the kriging model is a global meta model containing polynomial terms, it yields results very similar to those of the 30-point linear model. It confirms that the design variables and objective function are linearly correlated; therefore, only $n+1$ sampling points are required for constructing a linear surrogate model where n is the number of design variables. Moreover, the optimal design results gave an output efficiency higher than the efficiency of the sampling models obtained from the experiment design. Table 5 introduces the performance characteristics of the turbine based on CFD simulation between the maximum efficiency of the fifth sampling solution and the newly optimized model, and the blade angles of such solutions are found in Tables 1 and 4, respectively. The turbine efficiency of the optimized model is 89.87%, which is 5.42% more than that of the fifth sampling point. The turbine of the optimized model is characterized by the operating of flow rate of 4.16 m^3/s, total head of 1.88 meters, and 3276.11 Nm for the torque. The turbine torque of the optimized model decreased by 3.72% less than that of the fifth

Table 4. Optimal results based on three surrogate model.

Index	Parameters	Linear surrogate model		KRG-MHs
		30 sampling	9 sampling	30 sampling
Objective function, $\min: 1-\frac{\eta(\beta)}{100}$	β_1 (deg)	10.00	10.00	10.00
	β_2 (deg)	20.00	20.00	20.00
	β_3 (deg)	30.00	30.00	30.00
	β_4 (deg)	40.00	40.00	40.00
	β_5 (deg)	25.00	25.00	25.00
	β_6 (deg)	45.00	45.00	45.00
	β_7 (deg)	55.00	55.00	55.00
	β_8 (deg)	65.00	65.00	65.00
Optimal design	η_f (%)	98.57	90.16	98.57
	η_{optCFD} (%)	89.87	89.87	89.87
Fifth model in Table 2	$\eta_{re.}$ (%)	85.00	85.00	85.00
Comparison (%)	η_{optCFD} & $\eta_{re.}$	5.42	5.42	5.42
Validation error (%)	η_f & η_{optCFD}	8.82	0.32	8.82

Table 5. Performance characteristics of turbine.

Model	τ (Nm)	Q (m^3/s)	H (m)	η_{CFD} (%)
Optimal design	3276.11	4.16	1.88	89.87
Maximum efficiency of sampling model (fifth model in Table 2)	3397.82	4.38	1.95	85.00

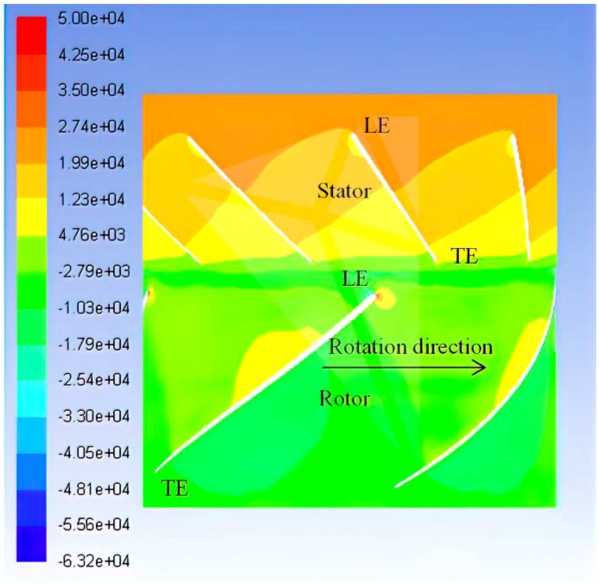

(a) Static pressure of the original design (Pa)

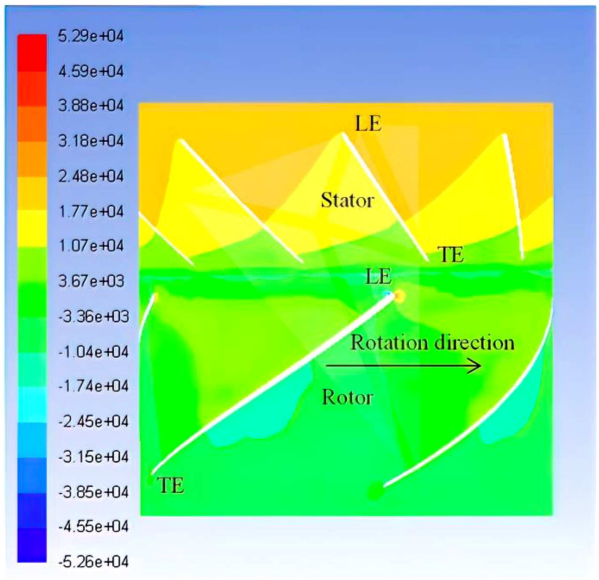

(b) Static pressure of the new design (Pa)

Figure 8. Pressure distribution in the blade tip domain of the stator-rotor.

sampling point. It should be noted that all of the torque, flow rate, and total head affect the turbine performance.

The optimal design of the blade angles of an axial flow turbine coupling with CFD at a VLH was proved to be an effective technique for improving the turbine performance. Figure 8 presents the results of different pressure characteristics of the stator-rotor section based on CFD analysis of the initial (fifth model in Table 1) and newly optimized models. Under the same operating conditions, the pressure distribution for the optimal design blade angles, compared to the original design illustrated in Figure 8(a), was improved (Figure 8(b)). Clearly, the pressure distribution around the center area of the original runner blade was less uniform than that of the new design. The pressure fluctuation on the leading and trailing edges of the guide vane and runner blades also decreased when using the optimal design.

6. Conclusions

The present study presented a simplified blade angle design of a VLH axial flow turbine using a surrogate-based optimization to reach the maximum efficiency of the turbine. The assigned design variables including the blade angles between the guide vanes and runner blades were positioned on the leading and trailing edges of the hub and blade tip. The LHS method was used in the experiment design with 30 sampling points of blade angles, and the LES turbulence model was simulated to analyze the flow in the turbine. According to the datasets of CFD results, the turbine efficiency was evaluated in the case of the correlation between the objective function and blade angles of the sampling points. Several optimizers were employed to tackle the proposed optimization problem and to evaluate their performance. In addition, three surrogate models including 30-point, 9-point linear models, and kriging were taken into account in this study. According to the findings, the linear surrogate model exhibited the best function since only $n + 1$ training points with n being the total number of design variables were required. The objective function was validated based on the error between the results of CFD and linear surrogate model, which was 0.32%. The result of the optimum blade angles was determined at β_1-β_8 of 10°, 20°, 30°, 40°, 25°, 45°, 55°, and 65°, respectively. The maximum efficiency of the turbine reached 89.87% with a flow rate of 4.16 m^3/s and total head of 1.88 meters.

Surrogate-based optimization was presented to design the blade angles of the guide vane and runner blade of the VLH axial flow turbine, which is very effective and can be applied to design other new blades. Since the objective function is linear, the more challenging design concept for such a turbine is how to accurately assign the best lower and upper bounds of the angles to obtain the highest possible efficiency.

Acknowledgments

The authors are grateful for the support received from the Thailand Research Fund (RTA6180010).

Nomenclature

Acronyms

Dia.	Diameter (m)
exp.	Experiment

min.	Minimum

Variables

D	Runner diameter (m)
D_h	Hub diameter (m)
H	Total head (m)
L_i	Lower bound
Q	Volume flow rate (m^3/s)
rand	Random
U_i	Upper bound
g	Gravitational acceleration (m/s^2)
β_i	Angles (degree)
τ	Torque (Nm)
η	Turbine efficiency
η_{CFD}	CFD turbine efficiency
η_f	Turbine efficiency of Surrogate model
η_{optCFD}	Optimization turbine efficiency
η_{re}	Reference turbine efficiency

References

1. Yang, W., Wu, Y., and Liu, S. "An optimization method on runner blades in bulb turbine based on CFD analysis", *Sci. China Technol. Sci.*, **54**(2), pp. 338–344 (2011).
2. Patel, V.A., Jain, S.V., Motwani, K.H., et al. "Numerical optimization of guide vanes and reducer in pump running in turbine mode", *Procedia Eng.*, **51**, pp. 797–802 (2013).
3. Ge, X., Feng, Y., Zhou, Y., et al. "Optimization study of shaft tubular turbine in a bidirectional tidal power station", *Adv. Mech. Eng.*, **2013**, pp. 1–9 (2013).
4. Amano, R.S. and Abbas, A. "Optimization of intake and draft tubes of a Kaplan micro hydro-turbine", *in 15th International Energy Conversion Engineering Conference*, Atlanta, GA (2017).
5. Ameen, A., Ibrahim, Z., Othman, F., et al. "Water flow stabilization using submerged weir for draft-tube reaction hydraulic turbine", *Sci. Iran.*, **27**(1), pp. 159–176 (2020).
6. Chakrabarty, S., Sarkar, B.K., and Maity, S. "CFD analysis of the hydraulic turbine draft tube to improve system efficiency", *MATEC Web Conf.*, **40** (2016).
7. Mulu, B.G., Cervantes, M.J., Devals, C., et al. "Simulation-based investigation of unsteady flow in near-hub region of a Kaplan turbine with experimental comparison", *Eng. Appl. Comput. Fluid Mech.*, **9**(1), pp. 139–156 (2015).
8. Wang, W., Zhang, L., Yan, Y., et al. "Large-eddy simulation of turbulent flow considering inflow wakes in a Francis turbine blade passage", *J. Hydrodyn. Ser B*, **19**(2), pp. 201–209 (2007).
9. Sutikno, P. and Adam, I.K. "Design, simulation and experimental of the very low head turbine with minimum pressure and free vortex criterions", *Int. J. Mech. Mech. Eng.*, **11**(1), pp. 9–16 (2011).
10. Cheng, Y., Lien, F.S., Yee, E., et al. "A comparison of large Eddy simulations with a standard $k-\varepsilon$ Reynolds-averaged Navier-Stokes model for the prediction of a fully developed turbulent flow over a matrix of cubes", *J. Wind Eng. Ind. Aerodyn.*, **91**(11), pp. 1301–1328 (2003).
11. Su, W.T., Li, F.C., Li, X.B., et al. "Assessment of Les performance in simulating complex 3D flows in turbomachines", *Eng. Appl. Comput. Fluid Mech.*, **6**(3), pp. 356–365 (2012).
12. Gupta, M.K. and Subbarao, P.M.V. "Development of a semi-analytical model to select a suitable airfoil section for blades of horizontal axis hydrokinetic turbine", *Energy Rep.*, **6**, pp. 32–37 (2020).
13. Langroudi, A.T., Afifi, F.Z., Nobari, A.H., et al. "Modeling and numerical investigation on multi-objective design improvement of a novel cross-flow lift-based turbine for in-pipe hydro energy harvesting applications", *Energy Convers. Manag.*, **203**, pp. 1-15 (2020).
14. Tingting, Y. and Yuan, Z. "Finite element analysis of stress, deformation and modal of head cover in axial-flow hydro-turbine", *J. Drain. Irrig. Mach. Eng.*, **38**(1), pp. 39–44 (2020).
15. Kolekar, N. and Banerjee, A. "A coupled hydro-structural design optimization for hydrokinetic turbines", *J. Renew. Sustain. Energy*, **5**, pp. 1–22 (2013).
16. Mastrogiannakis, I. and Vosniakos, G.C. "Exploring structural design of the Francis hydro-turbine blades using composite materials", *Facta Univ. Ser. Mech. Eng.*, **18**(1), pp. 43–55 (2020).
17. Bahrami, S., Tribes, C., Fellenberg, S., et al. "Multi-fidelity design optimization of Francis turbine runner blades", *IOP Conf. Ser. Earth Environ. Sci.*, **22**, pp. 1–10 (2014).
18. Mohammadi, M., Riasi, A., and Rezghi, A. "Design and performance optimization of a very low head turbine with high pitch angle based on two-dimensional optimization", *J. Braz. Soc. Mech. Sci. Eng.*, **42**(9), pp. 1–18 (2020).
19. Lyutov, A.E., Chirkov, D.V., Skorospelov, V.A., et al. "Coupled multipoint shape optimization of runner and draft tube of hydraulic turbines", *J. Fluids Eng.*, **137**(11), pp. 1–11 (2015).
20. Lazari, A. and Cattanei, A. "Design of off-statistics axial-flow fans by means of vortex law optimization", *J. Therm. Sci.*, **23**(6), pp. 505–515 (2014).
21. Juraeva, M., Ryu, K.J., and Song, D.J. "Optimum design of a saw-tooth-shaped dental air-turbine using design of experiment", *Int. J. Precis. Eng. Manuf.*, **15**(2), pp. 227–234 (2014).

22. Halder, P., Rhee, S.H. and Samad, A. "Numerical optimization of Wells turbine for wave energy extraction", *Int. J. Nav. Archit. Ocean Eng.*, **9**, pp. 11–24 (2017).

23. Chen, N., Zhang, H., Huang, W., et al. "Study on aerodynamic design optimization of turbomachinery blades", *J. Therm. Sci.*, **14**(4), pp. 298–304 (2005).

24. Castilho, L., Camacho, R.G.R., and Silva, E.R. "Optimized design of linear cascades for turbomachinery applications", *J. Braz. Soc. Mech. Sci. Eng.*, **38**, pp. 813–825 (2016).

25. Wang, W., Pei, J., Yuan, S., et al. "Application of different surrogate models on the optimization of centrifugal pump", *J. Mech. Sci. Technol.*, **30**(2), pp. 567–574 (2016).

26. Lu, H., Li, Q., and Pan, T. "Optimization strategy for an axial-flow compressor using a region-segmentation combining surrogate model", *J. Aerosp. Eng.*, **31**(5), (2018).

27. Giorgetti, S., Coppitters, D., Contino, F., et al. "Surrogate-assisted modeling and robust optimization of a micro gas turbine plant with carbon capture", in *Turbomachinery Technical Conference and Exposition*, Arizona, USA (2019).

28. Liu, L., Zhu, B., Bai, L., et al. "Parametric design of an ultrahigh-head pump-turbine runner based on multiobjective optimization", *Energies*, **10**, pp. 1–16 (2017).

29. Round, G.F., *Incompressible Flow Turbomachines*, Oxford, UK: Elsevier (2004).

30. Altimemy, M., Attiya, B., Daskiran, C., et al. "Mitigation of flow-induced pressure fluctuations in a Francis turbine operating at the design and partial load regimes-LES simulations", *Int. J. Heat Fluid Flow*, **79**, pp. 1–11 (2019).

31. Ramos, H.M., Simão, M., and Borga, A. "Experiments and CFD analyses for a new reaction microhydro propeller with five blades", *J. Energy Eng.*, **139**(2), pp. 109–117 (2013).

32. Gholami, A., Bonakdari, H., Akhtari, A.A., et al. "A combination of computational fluid dynamics, artificial neural network and support vectors machines model to predict flow variables in curved channel", *Sci. Iran.*, **26**(2), pp. 726–741 (2019).

33. Hosseini, F.M.M., Ebadi, T., Eslami, A., et al. "Investigation into geotechnical properties of clayey soils contaminated with gasoil using Response Surface Methodology (RSM)", *Sci. Iran.*, **26**(3), pp. 1122–1134 (2019).

34. Kurtuluş, E., Yıldız, A.R., Sait, S.M., et al. "A novel hybrid Harris hawks-simulated annealing algorithm and RBF-based metamodel for design optimization of highway guardrails", *Mater. Test.*, **62**(3), pp. 251–260 (2020).

35. Wansaseub, K., Sleesongsom, S., Panagant, N., et al. "Surrogate-assisted reliability optimisation of an aircraft wing with static and dynamic aeroelastic constraints", *Int. J. Aeronaut. Space Sci.*, **21**, pp. 723–732 (2020).

36. Reza, Z. "Dissipation and eddy mixing associated with flow past an underwater turbine", Master Thesis, Florida Atlantic university, USA (2010).

37. Ferro, L.M.C., Gato, L.M.C., and Falcão, A.F.O. "Design of the rotor blades of a mini hydraulic bulb-turbine", *Renew. Energy*, **36**(9), pp. 2395–2403 (2011).

38. Pholdee, N. "Performance enhancement of evolutionary optimisation using hybridsation concepts", PhD Thesis, Khon Kaen University, Thailand (2013).

39. Singh, P. and Nestmann, F. "Experimental investigation of the influence of blade height and blade number on the performance of low head axial flow turbines", *Renew. Energy*, **36**, pp. 272–281 (2011).

40. McKay, M.D., Beckman, R.J., and Conover, W.J. "A comparison of three methods for selecting values of input variables in the analysis of output from a computer code", *Technometrics*, **21**(2), pp. 239–245 (1979).

41. Kim, J.H., Choi, J.H., and Kim, K.Y. "Surrogate modeling for optimization of a centrifugal compressor impeller", *Int. J. Fluid Mach. Syst.*, **3**(1), pp. 29–38 (2010).

42. Karaboga, D. and Basturk, B. "On the performance of artificial bee colony (ABC) algorithm", *Appl. Soft Comput.*, **8**(1), pp. 687–697 (2008).

43. Socha, K. and Dorigo, M. "Ant colony optimization for continuous domains", *Eur. J. Oper. Res.*, **185**(3), pp. 1155–1173 (2008).

44. Storn, R. and Price, K. "Differential evolution - a simple and efficient heuristic for global optimization over continuous spaces", *J. Glob. Optim.*, **11**(4), pp. 341–359 (1997).

45. Merchaoui, M., Sakly, A., and Mimouni, M.F. "Particle swarm optimisation with adaptive mutation strategy for photovoltaic solar cell/module parameter extraction", *Energy Convers. Manag.*, **175**, pp. 151–163 (2018).

46. Mirjalili, S., Mirjalili, S.M., and Lewis, A. "Grey wolf optimizer", *Adv. Eng. Softw.*, **69**, pp. 46–61 (2014).

47. Mirjalili, S. "Moth-flame optimization algorithm: A novel nature-inspired heuristic paradigm", *Knowl.-Based Syst.*, **89**, pp. 228–249 (2015).

Biographies

Nantiwat Pholdee received his BEng and PhD in Mechanical Engineering from Khon Kaen University, Thailand, in 2008 and 2013, respectively. Currently, he is an Associate Professor at the Department of Mechanical Engineering, Khon Kaen University. His research interests include multidisciplinary design optimization,

surrogate-assisted optimization, meta-heuristic algorithms, and flight dynamic and control.

Weerapon Nuantong was born in Lom Sak, Phetchabun, Thailand in 1982. He received his BEng in 2006, MEng in 2009, and PhD in Mechanical Engineering from Khon Kaen University, Thailand in 2016. He is currently working at the Rajamangala University of Technology Isan, Khon Kaen Campus. His research interests include numerical simulations of fluid flow, heat transfer, and optimization design of turbine.

Sirivit Taechajedcadarungsri was born in Ubon Ratchatani, Thailand. He received his PhD in Engineering from New Jersey Institute of Technology, USA in 2002. His research interests include flow simulations, HVAC control systems, and robotic surgery.

Sujin Bureerat received his BEng in Mechanical Engineering from Khon Kaen University, Khon Kaen, Thailand in 1992 and PhD in Engineering from Manchester University, Manchester, UK in 2001. Currently, he is a Professor at the Department of Mechanical Engineering, Khon Kaen University. His research interests include multidisciplinary design optimization, evolutionary computation, aeroelastic design of aircraft structures, finite element analysis, agricultural machinery, and mechanical vibration.